processes

MDPI

Article

Crude Glycerol Hydrogenolysis to Bio-Propylene Glycol: Effect of Its Impurities on Activity, Selectivity and Stability

Martín N. Gatti [1,2], Francisco Pompeo [1,2], Nora N. Nichio [1,2] and Gerardo F. Santori [1,2,*]

[1] Centro de Investigación y Desarrollo en Ciencias Aplicadas (CINDECA), Facultad de Ciencias Exactas, Universidad Nacional de La Plata (UNLP)-CONICET, Calle 47, 257, La Plata 1900, Argentina; martin.gatti@ing.unlp.edu.ar (M.N.G.); fpompeo@quimica.unlp.edu.ar (F.P.); nnichio@quimica.unlp.edu.ar (N.N.N.)
[2] Facultad de Ingeniería, Universidad Nacional de La Plata (UNLP), Calle 1 esq. 47, La Plata 1900, Argentina
* Correspondence: santori@quimica.unlp.edu.ar

Abstract: The wide availability of crude glycerol and its low market price make this by-product of the biodiesel industry a promising raw material for obtaining high-value-added products through catalytic conversion processes. This work studied the effect of the composition of different industrial crude glycerol samples on the catalytic hydrogenolysis to 1,2-propylene glycol. A nickel catalyst supported on a silica–carbon composite was employed with this purpose. This catalyst proved to be active, selective to 1,2-propylene glycol and stable in the glycerol hydrogenolysis reaction in the liquid phase when analytical glycerol (99% purity) was employed. In order to determine the effect of crude glycerol composition on the activity, selectivity and stability of this catalyst, industrial crude glycerol samples were characterized by identifying and quantifying the impurities present in them (methanol, NaOH, NaCl and NaCOOH). Reaction tests were carried out with aqueous solutions of analytical glycerol, adding different impurities one by one in their respective concentration range. These results allowed for calculating activity factors starting from the ratio between the rate of glycerol consumption in the presence and in the absence of impurities. Finally, catalyst performance was evaluated employing the industrial crude glycerol samples, and a kinetic model based on the power law was proposed, which fitted the experimental results taking into account the effect of glycerol impurities. The fit allowed for predicting conversion values with an average error below 8%.

Keywords: biodiesel; crude glycerol; hydrogenolysis; 1,2-propylen glycol; nickel catalysts

check for updates

Citation: Gatti, M.N.; Pompeo, F.; Nichio, N.N.; Santori, G.F. Crude Glycerol Hydrogenolysis to Bio-Propylene Glycol: Effect of Its Impurities on Activity, Selectivity and Stability. *Processes* **2023**, *11*, 1731. https://doi.org/10.3390/pr11061731

Academic Editor: Yun Yu

Received: 20 May 2023
Revised: 30 May 2023
Accepted: 2 June 2023
Published: 6 June 2023

1. Introduction

Biomass compounds constitute an extensive set of platform molecules with a wide range of chemical functionality to obtain high-value-added products. Glycerol, a second-generation biomass compound, is obtained as a by-product of the biodiesel industry and allows for obtaining not only energy but also chemical products for industry [1].

Many catalytic processes, such as reforming, oxidation and esterification, can be employed in order to transform glycerol into other products of interest [2]. In this context, it has been extensively reported in the literature that glycerol hydrogenolysis allows for the production of bio-propylene glycol (1,2-PG), a product employed in the pharmaceutical, cosmetics, food industries and in the chemical industry in general. At present, 1,2-PG is obtained through a petrochemical process, so the production of 1,2-PG from glycerol is an environmentally friendly alternative, which, in the near future, could allow for decreasing the present dependence on fossil resources as raw materials [3].

The generation of 1,2-PG from glycerol is carried out through a two-step concerted mechanism [4,5]. In the first stage, glycerol is dehydrated to acetol (AcOH) and in the second stage, AcOH is hydrogenated to form 1,2-PG. In addition, cleavage reactions of C-C bonds in the glycerol molecule generate side products, such as methanol (MeOH) and ethylene glycol (EG). The consequent hydrogenolysis of 1,2-PG and EG produces terminal alcohols, such as 1-propanol (1-POH) and ethanol (EtOH). Finally, terminal alcohols 1-POH, EtOH and MeOH can also lead to the formation of gases, such as methane (MeO), ethane (EtO) and propane (PrO) (Scheme 1).

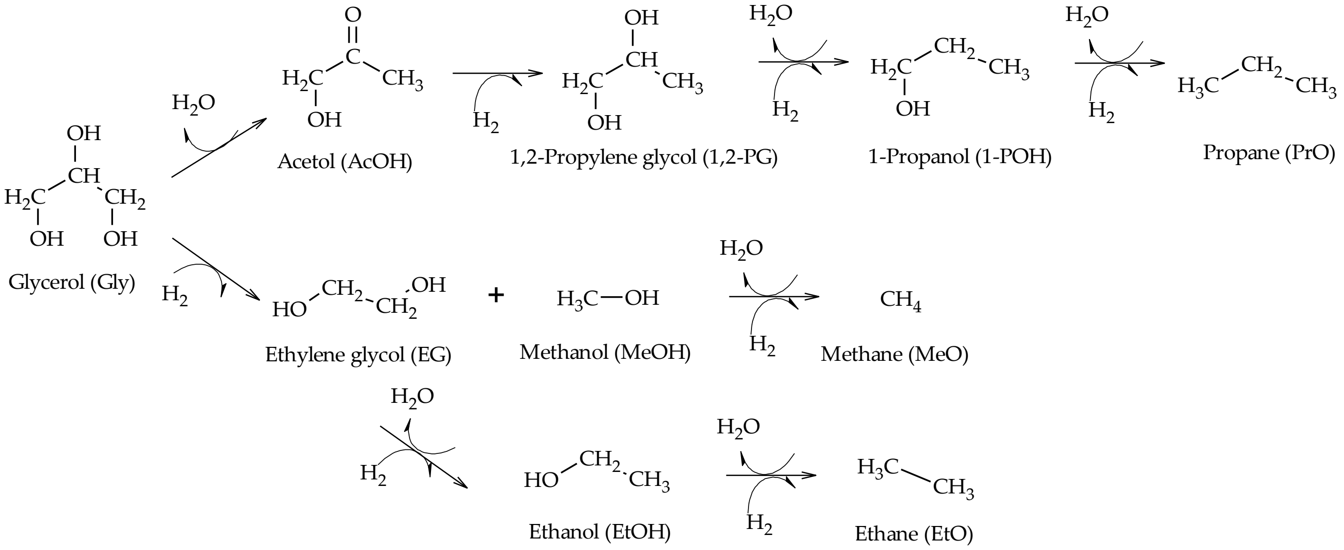

Scheme 1. Reactions involved in the dehydration–hydrogenation mechanism in glycerol hydrogenolysis.

It has been reported that catalytic supports play an important role in the formation of AcOH due to their acid–base properties, while metallic phases based on Ru [6], Pt [7], Pd [8], Cu [9–11] and Ni [12] intervene in the formation of 1,2-PG through AcOH hydrogenation.

In the course of time, reports on this topic have focused on the study of the operating variables, such as temperature, pressure, catalyst mass, pH and glycerol concentration, employed in the hydrogenolysis reaction in the liquid phase. The study of the operating variables assumes obtaining an optimal condition in which high yields to a 1,2-PG are reached without losing sight of the high costs associated with the reaction process.

The study of the operating variables has led to kinetic studies performed under liquid phase conditions employing batch reactors.

Different kinetic models have been developed, such as the power law models [6,8,9,13–16] and also the Langmuir–Hinshelwood models, considering one [9,17–19] or two types of active sites [20–24] and, in certain cases, the active site competition [17–19,21–24]. Values of energy activation of the overall reaction rate have been calculated [9,13,19] as well as activation energies for the dehydration and hydrogenation steps [24].

The power law models are the simplest ones and, therefore, very useful for reactor design since they employ simple mathematical equations to express the rate of reaction. Equation (1) express the rate of glycerol consumption ($-r_{gly}$) in terms of a kinetic coefficient (k_{gly}) and the concentration of reactants: glycerol (C_{gly}) and hydrogen (C_{H2}). Occasionally, the hydrogen concentration in the liquid phase is replaced by the H_2 partial pressure in the vapor phase in contact with the glycerol solution (P_{H2}).

$$-r_{gly} = -\frac{dC_{gly}}{dt} = k_{gly} C_{gly}^{\alpha} C_{H2}^{\beta} \tag{1}$$

In Equation (1), coefficients α and β are the partial orders of reaction with respect to glycerol and H_2, respectively.

Table 1 shows the kinetic information from the power law model obtained for different catalysts. In some of the models, experiments indicated that the glycerol consumption rate strongly depends on its concentration rather than on the concentration of H_2 in the liquid phase, being $\alpha > \beta$ [8,15], while in others, the reverse result was obtained [13,14].

Table 1. Catalysts and reaction conditions employed to obtain kinetic models based on the power law.

Catalyst	T (°C)	P_{H2} (MPa)	C_{gly} (wt.%)	Partial Orders of Reaction		Ref.
				α	β	
Pd-$CuCr_2O_4$	220	3–7	4.5–9.1	2.28	1.09	[8]
Co-ZnO	160–220	2–4	10–40	0.7355	0.5697	[15]
Cu-ZrO_2-MgO	160–220	2–5	10–40	0.6069	0.6955	[14]
Ru-Re/SiO_2	130	7.5	40	1	1 *	[6]
Cu/SiO_2	180–240	2–8	23.9–45.6	0.27	0.95	[13]
Cu-Zn-Cr-Zr	220–250	1–4	60–100	1	1 *	[20]
Cu/ZrO_2	175–225	2.5–3.5	2–8	0	1	[10]
Cu/MgO	190–230	3–6	20–60	1.20	n.d.	[9]
Cu-Ni/γ-Al_2O_3	180–220	3–6	20	1.02	n.d.	[11]

n.d.: not determined; α: partial order of reaction with respect to glycerol; β: partial order of reaction with respect to H_2. * Referred to P_{H2}.

Despite the efforts made, most articles considered the use of analytical glycerol as a starting reactant, employing a low concentration of glycerol in water (10–30 wt.%). In order to examine an operating condition at the industrial scale, it would be required to employ glycerol in concentrations similar to those of crude glycerol, which are well above that range (50–80 wt.%). In addition, crude glycerol contains a large number of impurities, among which inorganic bases can be found as well as sodium or potassium salts, residues of methanol (MeOH) and organic matter non-glycerol (MONG), such as free fatty acids and non-transesterified wastes of oils and fats [25–27]. The nature of these impurities and their concentration can have a different impact over the catalyst behavior in the production of 1,2-PG.

Cu/Al_2O_3 catalysts modified via impregnation with H_3BO_3 were evaluated employing pharmaceutical degree, technical and crude glycerol, obtaining that the catalyst performance was better when pharmaceutical glycerol was used as raw material, and the worst results were obtained employing crude glycerol samples. These results suggest that the impurities present in the crude glycerol can affect the catalyst performance [28]. Cu-Al catalysts resulted to be active and selective to 1,2-PG during 400 h of reaction in a continuous flow reactor in the liquid phase, operating with aqueous solutions of 20 wt.% refined glycerol at 220 °C and 2 MPa de N_2. The glycerol conversion obtained was 90% with a selectivity to 1,2-PG of 22–25%. When the tests were carried out with crude glycerol, 50% conversions were obtained with a 75% selectivity to 1,2-PG [29].

It has been reported that NaOH and KOH can be present in crude glycerol as they are employed as catalysts in biodiesel production. They can increase 1,2-PG production since they favor the first step of dehydration by means of OH^- ions. Nevertheless, in the case of NaOH, it has been reported that at high concentrations, it can lead to the formation of degradation products such as lactic acid [30]. If its presence is neutralized with the aid of inorganic acids, such as HCl or H_2SO_4, it leads to the formation of salts (NaCl and Na_2SO_4), respectively. The presence of these salts could also affect the catalytic performance [25,27,31]. Ru/TiO_2 catalysts were evaluated in the liquid phase condition using crude and refined glycerol containing Na_2SO_4 as an impurity. The results showed that glycerol conversion remained almost unchanged (46–42%) and also the selectivity to 1,2-PG (63–59%), indicating that the catalyst is resistant to the presence of this impurity in the crude glycerol [25].

Similar results were obtained using Cu-MgO catalysts employing crude glycerol and aqueous glycerol solutions with the addition of Na_2SO_4. Conversions between 85 and 90% were obtained employing crude and synthetic glycerol, maintaining a selectivity to 1,2-PG of 92% in all cases [31]. Recently, Rajkhowa et al. studied a Cu commercial catalyst, which was tested in a continuous flow reactor. The presence of NaCl as an impurity in crude glycerol provoked catalyst deactivation due to the effect of Cl^- in the sintering phenomena [27].

Since the transesterification of oils and fats leading to the formation of biodiesel uses short-chain alcohols, such as MeOH, the residues can also affect catalytic performance. There are different views on this matter. Gandarias et al. determined that MeOH is not suitable as a H_2-donor substance in the presence of Ni-Cu/γ-Al_2O_3 catalysts [32]. Other authors have reported that in the presence of MeOH and EtOH, the solubility of H_2 increases, which favors hydrogenation in the liquid phase [13]. As negative points, the formation of condensation products such as glyceryl ethers in the presence of MeOH and EtOH has been reported, which leads to obtaining low selectivity to 1,2-PG [33].

Finally, crude glycerol can contain free fatty acids and glycerides (mono-, di- or triglycerides). Catalytic surface can be fouled due to coke precursors generated by the presence of glycerides and can lead to the blocking of active sites [27].

The aim of this work is to study the effect of crude glycerol composition on the hydrogenolysis of glycerol to 1,2-PG using a Ni catalyst supported on a silica–carbon composite. Based on the results obtained, a power-law-based model is proposed to predict the conversion of crude glycerol of different natures when employed as a raw material in the hydrogenolysis process for the production of 1,2-PG.

2. Materials and Methods

2.1. Catalyst Synthesis and Characterization

A SiO_2-C (SC) composite was employed as catalyst support, prepared from TEOS and a phenolic resin. To do so, TEOS (SILBOND 40-AKZO Chemicals) was mixed with a phenol-formaldehyde liquid resin (RL 43003, ATANOR, Argentina) with a 1:1 mass ratio until an emulsion in ethanol medium was obtained. Then, pre-gelification occurred at room temperature for 24 h, and the gel was dried at 50 °C for another 24 h. Afterwards, complete polymerization occurred by heating to 180 °C for 3 h. Finally, a calcination step was carried out in absence of oxygen over 3 h at 1580 °C, leaving a high amount of residual carbon (SC).

The catalyst was prepared via incipient wetness impregnation using $Ni(CH_2COO)_2 \cdot 4H_2O$ (Sigma-Aldrich, Burlington, MA, USA) since its ease of decomposition prevents the support gasification. The nominal Ni content was 5 wt.%.

Then, it was dried in stove at 120 °C for 24 h and was finally activated in H_2 atmosphere (50 cm^3 min^{-1}) at 400 °C for 90 min (heating ramp 10 °C min^{-1}).

The samples were characterized using atomic adsorption spectroscopy (AAS), N_2 adsorption–desorption (BET), X-ray diffraction (XRD), potentiometric titration, isopropanol decomposition test reaction (IPA) and transmission electron microscopy (TEM).

The Ni content of the catalysts was determined using atomic absorption spectroscopy (AAS) (Spectrophotometer AA-6650 Shimadzu). The equipment utilized was an IL Model 457 spectrophotometer, with a single channel and double beam.

Adsorption–desorption measurements at −196 °C were performed for textural characterization. Surface area measurements, the Brunauer–Emmett–Teller (BET) multipoint method and textural analysis were utilized using Micromeritics ASAP 2020 equipment (Micromeritics Instrument Corporation, Norcross, GA, USA).

XRD patterns were recorded on a Philips 1729 powder diffractometer, using Cu Kα radiation (λ = 1.5418 Å, intensity = 20 mA and voltage = 40 kV).

Potentiometric titrations were performed using 0.05 g of support suspended in acetonitrile (Merck) and stirred for 3 h. Then, the suspension was titrated with 0.05 N n-butylamine (Carlo Erba) in acetonitrile using Metrohm 794 Basic Titrino apparatus with a double-junction electrode.

Transmission-electron microscopy (TEM) images were taken by means of a TEM JEOL 100 C instrument (JEOL Ltd., Tokyo, Japan), operated at 200 kV. The samples were suspended in 2-propanol and sonicated for 10 min in an ultrasonic bath prior to analysis. For the analysis, the particles were considered spherical, and the average diameter volume/area

(d_{va}) was estimated using Equation (2), where n_i is the number of particles with diameter d_i.

$$d_{va} = \frac{\sum n_i \cdot {d_i}^3}{\sum n_i \cdot {d_i}^2} \tag{2}$$

The particle size distribution histograms were obtained from micrographs employing the bright-field technique and counting about 200 particles per image.

2.2. Characterization of Crude Glycerol

To study the effect of impurities, different types (A, B, C, D and E) of crude glycerol were used, supplied by chemical plants located in the province of Buenos Aires, Argentina. They were characterized according to their density, pH and concentrations of glycerol, water, methanol, ash and non-glycerol organic matter (MONG).

The pH was determined using 1 g of crude glycerol dissolved in 50 mL of distilled water using a digital pH meter (Ohaus ST20, Greifensee, Switzerland) at room temperature.

Density was measured at room temperature employing a pycnometer (ASTM 891-95). Dilute crude glycerol samples were analyzed in a gas chromatograph to determine glycerol and methanol concentrations. For this purpose, a Shimadzu GCMS-QP505A instrument (Shimadzu Corporation, Tokyo, Japan) equipped with a 50 m 19091S-001 HP PONA capillary column and FID detector was used. The Karl-Fisher titrator (SI Analytics TitroLine Alpha 20 Plus, Xylem Analytics, Weilheim, Germany) was used to measure the water content according to ISO 760-1978. Finally, the ash content was measured by burning 1 g of crude glycerol in a muffle at 750 °C for 3 h (ISO 2098-1972). Organic matter non-glycerol (MONG) content was calculated, as shown in Equation (3).

$$\text{MONG (wt.\%)} = 100 - \text{glycerol content (wt.\%)} - \text{ash content (wt.\%)} - \text{water content (wt.\%)} \tag{3}$$

2.3. Catalytic Activity

The hydrogenolysis reactions were carried out with a BR-100 (Berghof, Eningen, Germany) high-pressure stainless-steel batch reactor of 100 cm^3. The magnetic stirring was fixed at 1000 rpm in order to ensure the kinetic control conditions.

The catalyst was reduced ex situ in H_2flow (50 $cm^3\ min^{-1}$) at 400 °C over 90 min (heating rate of 10 °C min^{-1}). The catalysts were cooled down to room temperature under hydrogen stream and immediately transferred to the reactor containing the glycerol aqueous solution (30–80 wt.% of glycerol and 0.08–0.24 catalyst/glycerol mass ratios). Then, the reactor was closed, purged and pressurized with pure H_2 (Air Liquide, 99.99%) at the desired pressure (1–2 MPa). Afterwards, heating was started (6 °C min^{-1}) and when the reactor was at the set temperature (220–260 °C), stirring began.

As glycerol hydrogenolysis reactions produce both gas and liquid products, no intermediate sampling was performed in any of the batch runs. In this sense, to obtain the concentration–time profiles at different temperatures and pressures, the reactions were performed individually and stopped at various predetermined times to conduct the analyses of gas and liquid phase products.

After reaction, the reactor was cooled to ambient temperature and the gas and liquid products were analyzed. A Shimadzu GC-8A (Shimadzu Corporation, Tokyo, Japan) gas chromatograph equipped with a thermal conductivity detector (TCD), and a Hayesep D 100–120 column was employed for the analysis of gaseous products. Liquid products were analyzed employing a Shimadzu GCMS-QP505A (Shimadzu Corporation, Tokyo, Japan) gas chromatograph, equipped with a 50 m 19091S-001 HP PONA capillary column (Agilent J&W, Santa Clara, CA, USA) and FID and Msdetectors (Shimadzu Corporation, Tokyo, Japan).

The total glycerol conversion (X_T) was determined as follows:

$$X_T = \frac{\text{moles of consumed glycerol}}{\text{moles of initial glycerol}} \cdot 100\ \% \tag{4}$$

The conversion of glycerol to liquid products (X_L) was determined as follows:

$$X_L = \frac{\sum \text{moles of carbon in liquid products}}{\text{moles of carbon in initial glycerol}} \cdot 100\ \% \quad (5)$$

The conversion of glycerol to gaseous products (X_G) was determined as follows:

$$X_G = X_T - X_L \quad (6)$$

The selectivity to liquid products was defined as:

$$\text{Selectivity of liquid product } (\%) = \frac{\text{moles of carbon in specific product}}{\sum \text{moles of carbon in liquid products}} \cdot 100\ \% \quad (7)$$

The selectivity to gaseous products was defined as:

$$\text{Selectivity of gaseous product } (\%) = \frac{\text{moles of carbon in specific product}}{\sum \text{moles of carbon in gaseous products}} \cdot 100\ \% \quad (8)$$

In order to quantify deactivation, the activity definition according to Equation (9) was employed:

$$\text{Activity } (\%) = \frac{\text{glycerol conversion in the reaction cycle}}{\text{glycerol conversion in the first reaction cycle}} \cdot 100\ \% \quad (9)$$

The carbon balance was calculated employing Equation (9):

$$\text{Carbon balance } (\%) = \frac{\sum \text{moles of carbon in products}}{3 \cdot \text{moles of initial glycerol}} \cdot 100\ \% \quad (10)$$

The accuracy of the measured values was within 5%, and the experiments could be reproduced with a relative error of 10%. The carbon balance for all runs was close to 98%.

2.4. Kinetic Model

In Scheme 1, it can be observed that the formation of 1,2-propylene glycol (1,2-PG), ethylene glycol (EG) and methanol (MeOH) proceeds through the reaction between glycerol (Gly) and hydrogen (H_2). Ethanol (EtOH) and propanol (1-POH), however, are produced through the hydrogenolysis of EG and 1,2-PG, while the methane (MeO), ethane (EtO) and propane (PrO) gases come from the hydrogenolysis of MeOH and EtOH. In these cases, the formation equations can be combined to be glycerol and H_2 dependant.

Taking these considerations into account, a kinetic model based on the power law was proposed to express the overall rate of glycerol consumption ($-r_{gly}$) using Equation (1).

With this model, the formation rates of each compound j (r_j) were expressed in terms of the molar concentration of glycerol (C_{gly}) and the molar concentration of H_2 (C_{H2}) (Equation (11)).

$$r_j = \frac{dC_j}{dt} = k_j C_{gly}^{\alpha j} C_{H2}^{\beta j} \quad (11)$$

In Equation (11), coefficients α_j and β_j are the partial orders with respect to glycerol and H_2, while k_j is the kinetic coefficient of the rate of formation of compound j.

In all cases, the molar concentration of H_2 in liquid phase was estimated employing Henry's constant (H_{H2}) considering the solubility of H_2 in water and was corrected by temperature according to van't Hoff's equation (Equation (12)).

$$H_{H2}\ (T) = H_{H2}(T_o) \exp \left[\frac{\Delta H_{sol}}{R} \left(\frac{1}{T} - \frac{1}{T_o} \right) \right] \quad (12)$$

The values of H_{H2} (T_o) and ΔH_{sol} at T_o = 298 K were obtained from the NIST (National Institute of Standards and Technology) database.

From the concentration–time and H_2 concentration–partial pressure profiles for each compound j, the initial formation rates (r_j) were measured, and the partial orders of reaction with respect to glycerol (α_j) and H_2 (β_j) were estimated using simple linear regression.

Then, with the concentration–temperature profiles, the kinetic coefficients (k_j) were estimated, and the apparent activation energy (Ea_j) and the pre-exponential factor (k_{oj}) were estimated, using the Arrhenius law (Equation (13)) and its linearization (Equation (14)).

$$k_j = k_{oj} e^{-E_{aj}/RT} \tag{13}$$

$$\ln(k_j) = \ln(k_{oj}) - \frac{E_{aj}}{RT} \tag{14}$$

From the study of the effect of impurities of crude glycerol, the rate of glycerol consumption ($-r_{gly}$) was modified by an individual activity factor (a_i) to obtain the rate of glycerol consumption in the presence of a given impurity ($-r_{gly}{}'$), according to Equation (15).

$$(-r_{gly}{}') = a_i(-r_{gly}) \tag{15}$$

The individual activity factors (a_i) are an exclusive function of the concentration of each impurity (C_i) and were calculated from Equation (15). Then, their characteristic parameters (n, k_i, K_i) were obtained from the adjustment of Equation (16), where it was verified that when C_i = 0, a_i = 1 and ($-r_{gly}{}'$) = (r_{gly}). The ± sign depends on the positive (+) or negative (−) effect of each particular impurity on the rate of glycerol consumption.

$$a_i = 1 \pm \frac{k_i C_i^n}{1 + K_i C_i^n} \tag{16}$$

From the individual activity factors, the total activity factor (a_T) was calculated, which takes into account all the impurities present in crude glycerol (Equation (17)).

$$a_T = 1 + \sum (a_i - 1) \tag{17}$$

Based on the total activity factor, the rate of glycerol consumption in the presence of all impurities was expressed according to Equation (18).

$$(-r_{gly}{}') = a_T k_{gly} C_{gly}^{\alpha} C_{H2}^{\beta} \tag{18}$$

Equation (18) was integrated in order to obtain the conversion of different qualities of crude glycerol and to contrast the results of the model with those obtained experimentally.

3. Results and Discussion

3.1. Catalysts and Support Characterization

In a previous study, we reported the synthesis and use of the SC composite as a support for Ni catalysts in glycerol hydrogenolysis. The textural and acid–base properties of this material remained unchanged under the pressure and temperature conditions of the hydrogenolysis reaction, proving that the SC composite is a stable support. The textural and physicochemical properties of the SC support and Ni/SC catalysts are shown in Table 2.

Through atomic absorption spectroscopy (AAS), the Ni content was determined to be approximately 4.5 wt.%, very close to the nominal content of 5 wt.%, for the fresh and used Ni/SC samples.

The N_2adsorption–desorption (BET) results showed specific surface areas of the 200 m^2 g^{-1} order for both the SC support and the Ni/SC catalyst. Both present type IV isotherms with H3 hysteresis loops, characteristic of mesoporous materials with a low contribution of micropores. The N_2 adsorption–desorption isotherms for SC and Ni/SC are shown in the Supplementary Materials (Figure S1).

Table 2. Textural and physicochemical properties of the SC support and Ni/SC catalysts.

Sample	**AAS**	**BET**						**Potentiometric Titration**		**TEM**	
	Ni [a]	**S_{BET}** [b]	**V_p** [c]	**Micropores**		**Mesopores**		**E_i** [h]	**NS** [i]	**d_{va}** [j]	**D** [k]
				S_{micro} [d]	**V_{micro}** [e]	**S_{meso}** [f]	**V_{meso}** [g]				
SC	-	208	0.48	55	0.02	153	0.46	12	0.18	-	-
Ni/SC	4.46	207	0.43	59	0.03	148	0.40	30	0.22	20.1	4.8
Ni/SC *	4.32	191	0.39	48	0.03	143	0.36	26	0.19	22.2	4.4

[a] Ni mass content (wt.%) [b] Specific surface area (m^2 g^{-1}) [c] Total pore volume (cm^3 g^{-1}) [d] Specific surface area of micropores (m^2 g^{-1}) [e] Total pore volume of micropores (cm^3 g^{-1}) [f] Specific surface area of mesopores (m^2 g^{-1}) [g] Total pore volume of mesopores (cm^3 g^{-1}) [h] Initial potential (mV) [i] Number of acid sites (mmol g^{-1}) [j] Average diameter volume/area (nm) [k] Dispersion (%). * Used in 3 reaction tests of 2 h each at 260 °C and 2 MPa of H_2.

The acid–base properties of SC and Ni/SC were determined via potentiometric titration with n-butylamine, since this technique is the most appropriate one for carbon-based materials. The techniques employing pyridine adsorption present difficulties caused by the presence of these materials' micropores.

Table 2 shows the values of acidic strength (E_i) and total number of acid sites (NS), while the titration curves are shown in the Supplementary Materials (Figure S2). From these results, it is possible to observe that the SC support has strong acid sites ($0 \text{ mV} < E_i < 100 \text{ mV}$) with the total number of sites in the order of 0.20 mmol g^{-1} [34]. The nature of the acidity of the support comes from oxygenated surface groups ($-COOH$, $-C{=}O$, $-COH$) that confer Lewis-type acidity [35], which allows it to catalyze the dehydration reaction of glycerol to acetol (AcOH), the main intermediate in the formation of 1,2-PG.

The results in Table 2 show that the fresh and used Ni/SC catalysts preserve the surface acidity of the support and the total number of acid sites.

The transmission electron microscopy (TEM) analysis revealed the presence of Ni particles in the order of 20 nm, corresponding to 4.8% metal dispersion for the fresh catalyst and 22 nm and 4.4% dispersion for the used catalyst. TEM micrographs of the fresh and used Ni/SC catalysts with their corresponding particle size distributions are shown in the Supplementary Materials (Figure S3).

The XRD spectra of the SC support and fresh and used Ni/SC catalysts are shown in the Supplementary Materials (Figure S4). The results indicate that there are no modifications in the structure of the SC support or in the fresh and used Ni/SC catalysts either.

The structural stability of the catalyst was also corroborated by the catalytic stability of the glycerol hydrogenolysis reaction in the liquid phase.

3.2. Characterization of Industrial Crude Glycerol Samples

The characterization of crude glycerol coming from different biodiesel industries located in the Province of Buenos Aires, Argentina, is shown in Table 3.

Table 3. Physicochemical properties and composition of crude glycerol samples.

Sample	**pH**	**Density (g mL^{-1})**	**Composition (wt.%)**				
			Glycerol	**H_2O**	**Ashes**	**MeOH**	**MONG** [f]
A	6.0	1.2783	77.39	19.30	0.71 [a]	0.29	2.31
B	6.0	1.2574	79.26	11.00	4.00 [b]	2.00	3.74
C	9.0	1.1367	52.66	18.00	2.70 [c]	10.48	16.16
D	6.0	1.2080	77.20	10.97	6.00 [d]	0.00	5.83
E	12.0	1.1560	77.59	0.24	3.22 [e]	6.28	12.67

[a] NaCl [b] NaCOOH [c] NaOH [d] NaCl [e] NaOH. [f] the content of MeOH (wt.%) was not included in the total content of MONG (wt.%).

Sample A was provided by the Y-TEC (YPF S.A. + CONICET) division, located in the town of Berisso, province of Buenos Aires, Argentina. Samples B and C were supplied by the Oleomud S.A. company, located in the locality of Florencio Varela, province of Buenos Aires, Argentina. Samples D and E were supplied by the AriparBio industrial plant of AriparCereales S.A., located in Daireaux, province of Buenos Aires, Argentina.

The results in Table 3 indicate that samples C and E have not been neutralized given their pH > 7, so that their ash content is based on the remaining NaOH from the biodiesel production process. Samples A, B and D show a pH = 6, which indicates that they have been neutralized post-reaction and their ashes derive from the salts formed by neutralization. In this regard, A and D were neutralized with HCl, which explains the presence of NaCl in these samples, while B was neutralized with HCOOH, which explains the presence of NaCOOH.

In all cases, the water content does not exceed 20 wt.% and the glycerol content is approximately 80 wt.% for all the samples, except for glycerol C, in which the concentration is lower in the order of 60 wt.%. For this sample, the lower glycerol content agrees with the lower density value found among the different samples.

With respect to MeOH, the maximum content found was 10 wt.% in sample C, while MeOH was not detected in sample D.

MONG includes the non-glycerol organic matter formed by a set of free fatty acids, oils, fats and phospholipids that come from the transesterification reaction in biodiesel production. Methanol is also included, but its content can be discounted since it is already quantified independently. The results in Table 3 indicate that the MONG content reaches a maximum concentration of 16 wt.% in sample C.

3.3. Effect of Impurities over the Catalytic Activity

First, reaction tests were carried out with aqueous solutions of analytical glycerol (99.99%), individually adding the different impurities present in the crude glycerol (H_2O, MeOH, NaOH, NaCl and NaCOOH). MONG represents a wide variety of organic compounds of different natures, such as glycerides, phospholipids and fatty acids, among others. As they cannot be associated to one specific chemical compound, they were not considered in this study.

Table 4 shows the composition of the impurities in the crude glycerol samples expressed in terms of the molar ratio of each impurity with respect to glycerol (mol mol^{-1}). The study of the effect on the catalytic activity of each impurity was performed individually and in the concentration range shown in Table 4.

Table 4. Composition of the impurities of crude glycerol samples in terms of the glycerol-based molar ratio.

Sample	Glycerol-Based Molar Ratio (mol mol^{-1})				
	H_2O	NaOH	NaCOOH	NaCl	MeOH
A	1.2746	-	-	0.0144	0.0108
B	0.7093	-	0.0683	-	0.0725
C	1.7471	0.1179	-	-	0.5722
D	0.7263	-	-	0.1222	-
E	0.0158	0.0955	-	-	0.2327

3.3.1. Effect of H_2O

Figure 1a shows conversion as a function of the water/glycerol molar ratio (H_2O/Gly) in the reaction mixture. The results indicate that conversion remains invariant with the increase in the H_2O/Gly molar ratio between 0 and 2.11, which is equivalent to 0 and 28 wt.%.

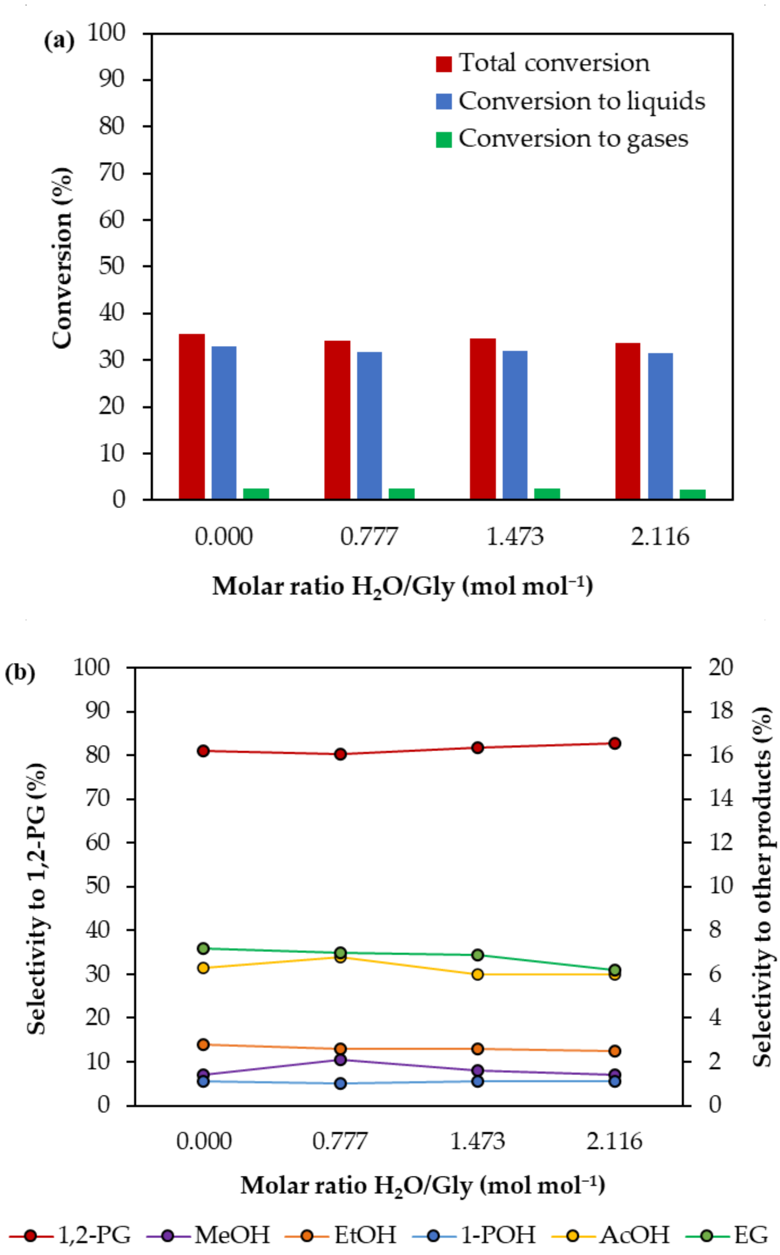

Figure 1. (**a**) Conversion as a function of the H_2O/Gly molar ratio. (**b**) Selectivity to liquid products as a function of the H_2O/Gly molar ratio. Reaction conditions: 30 wt.% glycerol solution, 260 °C, 2 MPa, 2 h, $m_c/m_{gly} = 0.24$.

It has been reported that in the presence of $Rh_{0.02}Cu_{0.4}/Mg_{5.6}Al_{1.98}O_{8.57}$ catalysts, glycerol conversion falls from 91% to 69% when the water content increases from 0 wt.% to 40 wt.%, using ethanol as a solvent (180 °C, 2 MPa of H_2) [36]. For the same increment in water content, similar results were obtained employing Ni/Ce-Mg catalysts, with a decrease in glycerol conversion from 80% to 43%, even when selectivity to 1,2-PG remained almost unchanged (56–58%) [37]. The results in Figure 1a show that the conversion remains almost constant, which could be assigned to the hydrophobic characteristics of the support protecting the active sites from the hydrolytic attack by water. Figure 1b, on the other hand, shows that the selectivity to 1,2-PG is also kept constant in this molar range of H_2O/Gly.

3.3.2. Effect of NaOH

Figure 2a shows the glycerol conversions as a function of the sodium hydroxide/glycerol (NaOH/Gly) molar ratio in the reaction mixture. An increase in the total glycerol conversion from 35 to 100% is observed when the NaOH/Gly molar ratio increases from 0 to 0.09, respectively.

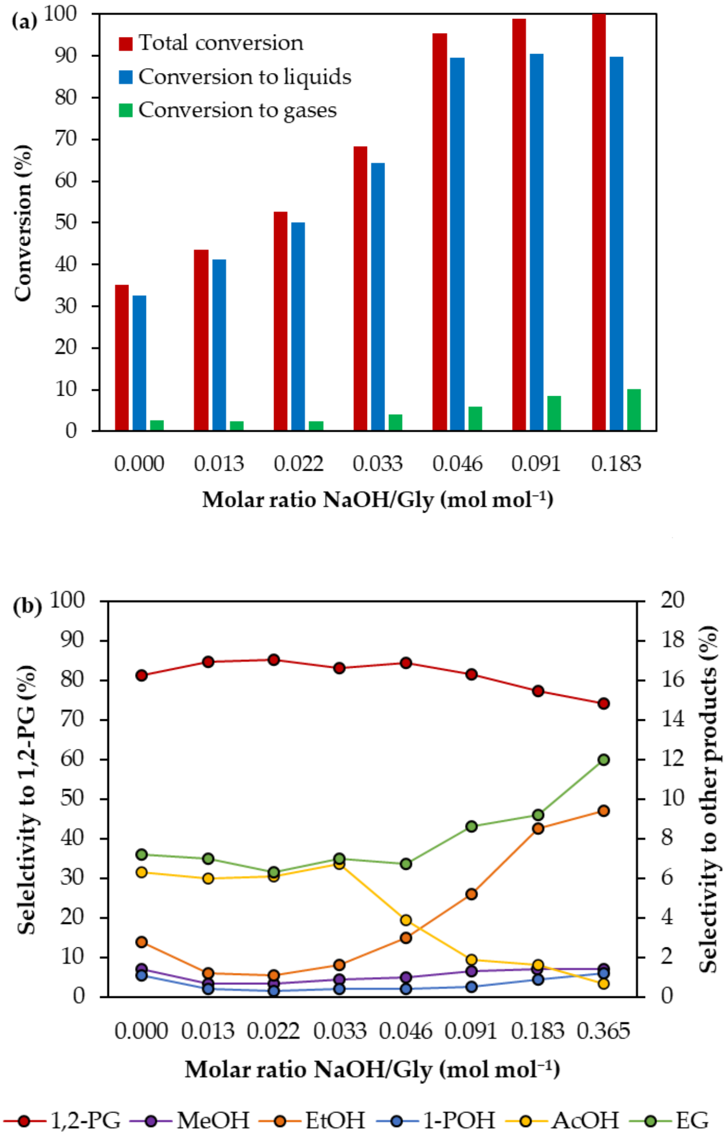

Figure 2. (**a**) Conversion as a function of the NaOH/Gly molar ratio. (**b**) Selectivity to liquid products as a function of the NaOH/Gly molar ratio. Reaction conditions: 30 wt.% glycerol solution, 260 °C, 2 MPa, 2 h, m_c/m_{gly} = 0.24.

Figure 2b shows that, once the complete conversion of glycerol is achieved, an increase in the NaOH content produces a slight decrease in the selectivity to 1,2-PG from 84% to 77% and, consequently, a higher selectivity to EG and EtOH also occurs. Kunosoki et al. reported that EtOH can be produced via the hydrogenolysis of 1,2-PG [38]. Magliano et al. indicated that, although EtOH can also be produced via the hydrogenolysis of AcOH, from a thermodynamic point of view, the hydrogenolysis of 1,2-PG is favored [39].

Feng et al. [40] studied a Ru/TiO_2 catalyst at 170 °C and 3 MPa of H_2 in the presence of LiOH, NaOH, $Na_2CO_3$and Li_2CO_3. Their results showed that the presence of these bases favored the conversion of glycerol in the 66–89% range, with an almost constant selectivity to 1,2-PG (83–89%), independently of the type of base added. These authors remarked that the presence of these bases provides OH^-, favoring the formation of glyceraldehyde from glycerol through a dehydrogenation step. Similar results were obtained using a $CuCr_2O_4$ catalyst [41].

3.3.3. Effect of NaCOOH

Figure 3a shows the glycerol conversions as a function of the molar ratio of sodium formate to glycerol (NaCOOH/Gly). The results show an increase in total glycerol conversion, from 35% to 98%, when the NaCOOH/Gly molar ratio increases from 0 to 0.107. Figure 3b shows that the selectivity to 1,2-PG is not affected.

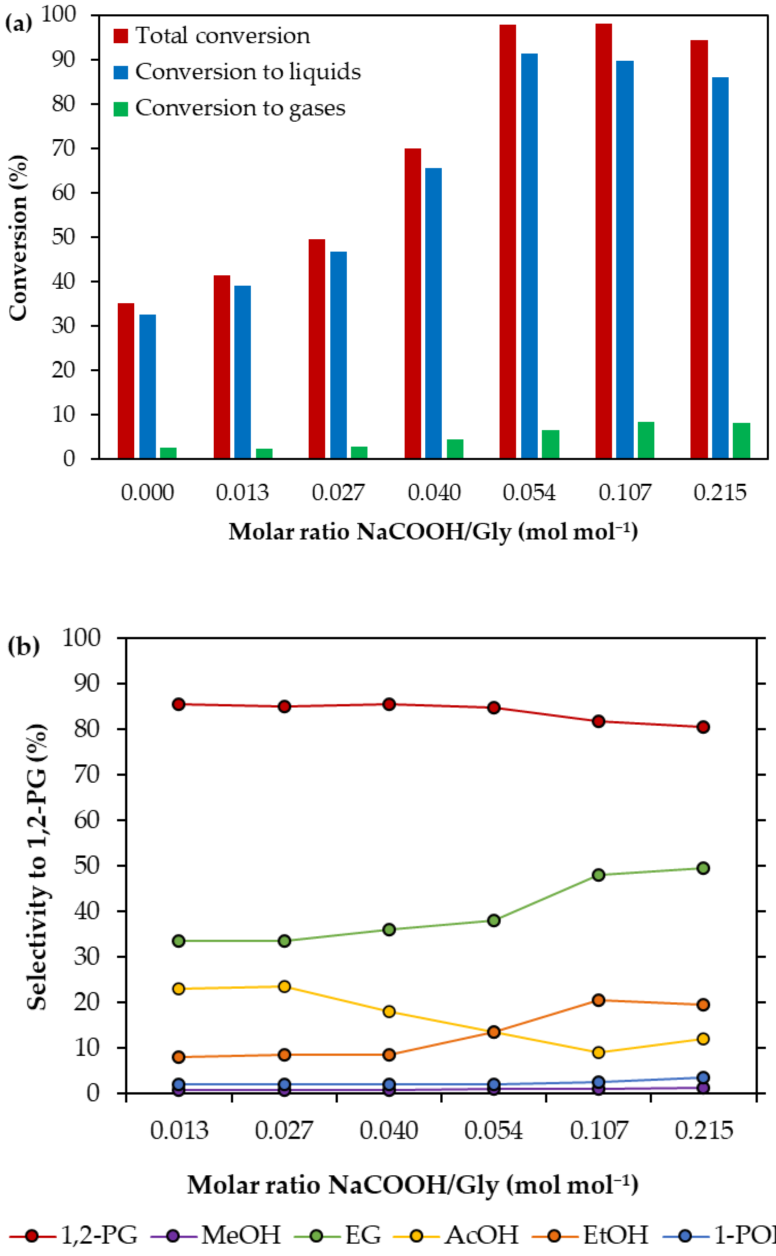

Figure 3. (**a**) Conversion as a function of the NaCOOH/Gly molar ratio. (**b**) Selectivity to liquid products as a function of the NaCOOH/Gly molar ratio. Reaction conditions: 30 wt.% glycerol solution, 260 °C, 2 MPa, 2 h, $m_c/m_{gly} = 0.24$.

Even though sodium formate is not a base, its equilibrium in aqueous solution generates OH^- ions due to the hydrolysis of the formate ion, as shown in Equations (19) and (20).

$$NaCOOH \rightarrow Na^+ + HCOO^- \quad (19)$$

$$HCOO^- + H_2O \leftrightarrow HCOOH + OH^- \quad (20)$$

Lahr et al. [17] tested commercial Ru/C catalysts in the presence of CaO and $CaCO_3$. Their results determined that increasing the OH^- ion concentration led to an increase in glycerol conversion with an increase in the selectivity to EG.

3.3.4. Effect of NaCl

Figure 4a shows the glycerol conversion as a function of the sodium chloride/glycerol (NaCl/Gly) molar ratio. A decrease in activity can be observed, from 35% to 12% of glycerol conversion, as the NaCl/Gly molar ratio increases from 0 to 0.125. These results are in agreement with those obtained by Rajkhowa et al. who studied the deactivation phenomena due to the presence of Cl^- ions of a commercial Cu catalyst, evaluated in the hydrogenolysis of glycerol at 230 °C and 7 MPa H_2 and using a trickle-bed reactor. The presence of these Cl^- ions in the reaction medium produced a deactivation of the catalyst due to sintering via the incorporation of Cl^- into the Cu particles [27]. In turn, Boga et al. studied Pt/Al_2O_3 catalysts in the aqueous reforming of crude glycerol at 225 °C and 2.9 MPa of N_2. They found that NaCl causes a drop in glycerol conversion and a decrease in H_2 production [42]. Similar results were obtained by Lehnert and Claus, who assigned the loss of activity in Pt/Al_2O_3 catalysts to the presence of inorganic salts in the crude glycerol, including NaCl, which caused a blockage of active sites [43].

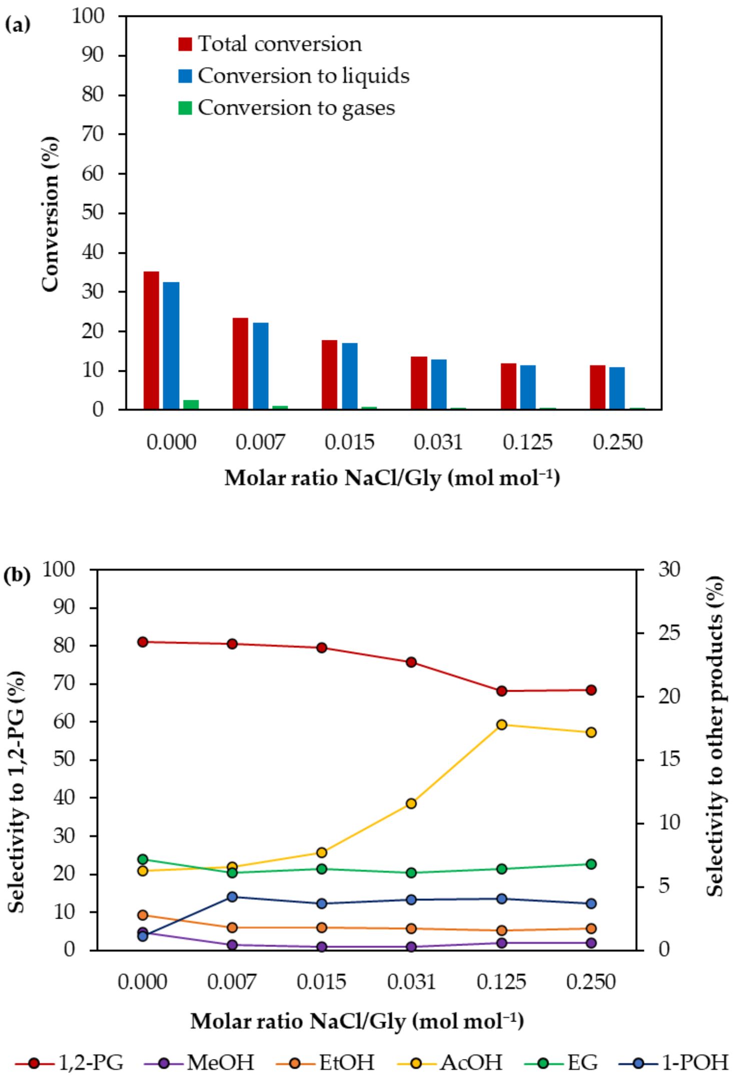

Figure 4. (**a**)Conversion as a function of the NaCl/Gly molar ratio. (**b**) Selectivity to liquid products as a function of the NaCl/Gly molar ratio. Reaction conditions: 30 wt.% glycerol solution, 260 °C, 2 MPa, 2 h, m_c/m_{gly} = 0.24.

Figure 4b shows that there is also a decrease in the selectivity to 1,2-PG, from 80 to 68%, for NaCl/Gly molar ratios higher than 0.031, accompanied by an increase in the selectivity to AcOH from 10 to 18%, respectively. This would indicate that NaCl could block the metal site and, thus, decrease the hydrogenation capacity of the catalyst.

3.3.5. Effect of MeOH

Figure 5a shows the decrease in glycerol conversion from 35 to 24%, when the methanol/glycerol molar ratio (MeOH/Gly) is increased from 0 to 0.211. However, no significant changes can be observed in the selectivity to 1,2-PG (Figure 5b), which remains at approximately 80%.

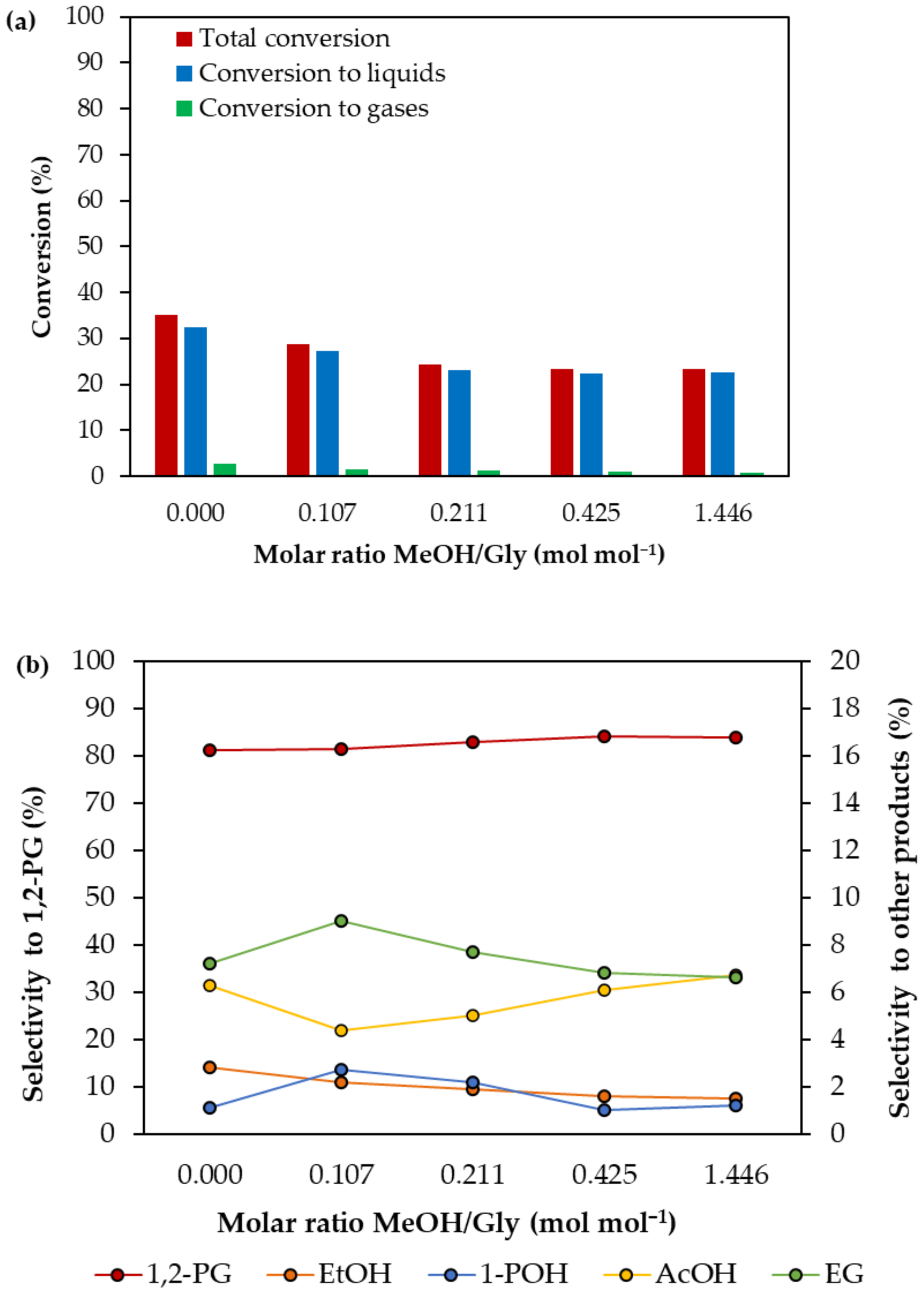

Figure 5. (**a**) Conversion as a function of the MeOH/Gly molar ratio.(**b**) Selectivity to liquid products as a function of the MeOH/Gly molar ratio. Reaction conditions: 30 wt.% glycerol solution, 260 °C, 2 MPa, 2 h, $m_c/m_{gly} = 0.24$.

Even though it has been reported in the literature that MeOH is a H_2-donor substance [44] and a positive effect on the hydrogenation stage could be thought of, it should also be considered that glycerol and methanol can compete for the same active sites in the hydrogenolysis reaction [26,32] and this could explain the decrease in activity at higher MeOH contents.

3.4. Catalytic Performance Using Industrial Crude Glycerol

3.4.1. Activity and Selectivity

The crude glycerol samples were tested in the hydrogenolysis reaction using 30 wt.% solutions at 260 °C and 2 MPa with a m_c/m_{gly} = 0.24 mass ratio. In Table 5, it is possible to observe that in all crude glycerol samples, although different conversions are achieved, all crude glycerol samples show selectivity values of 1,2-PG between 77 and 81% for glycerol conversions of ~30%.

Table 5. Results of the catalytic activity in the hydrogenolysis of crude glycerol using Ni/SC.

Sample	t (h)	X_T	X_G	X_L	Selectivity (%)					
					EtOH	AcO	1-POH	AcOH	EG	1,2-PG
R	2	35.1	2.6	32.5	2.8	0.1	1.1	6.3	7.2	81.1
A	2	24.0	0.9	23.1	0.9	0.3	0.5	7.7	6.4	84.2
	3	38.7	1.3	37.4	1.0	0.2	0.8	12.5	5.9	79.6
B	2	80.7	3.4	77.3	2.4	0.8	0.3	1.0	6.4	89.1
	0.5	29.9	1.8	28.1	3.0	1.7	0.5	7.1	10.0	77.7
C	2	87.8	3.9	83.9	2.0	1.1	0.3	5.0	5.3	86.3
	0.25	28.5	1.1	27.4	2.5	1.4	0.4	11.3	5.8	78.6
D	2	18.0	0.5	17.5	0.7	0.4	0.9	14.8	4.9	78.3
	4	32.4	0.8	31.6	1.1	0.8	2.0	10.9	3.9	81.3
E	2	97.6	5.0	92.6	1.8	1.4	0.4	1.1	5.4	89.9
	0.25	34.4	1.5	32.9	2.0	1.1	0.3	8.5	8.6	79.5

Reaction conditions A–E: 30 wt.% solution of crude glycerol, 260 °C, 2 MPa, 2 h, m_c/m_{gly} = 0.24. Reaction conditions R: 30 wt.% solution of analytical glycerol, 260 °C, 2 MPa, 2 h, m_c/m_{gly} = 0.24.

The highest conversion levels are obtained with glycerol B, C and E samples, while the lowest conversions are achieved with glycerol A and D samples.

Samples A and D have the same glycerol content, similar water content, low MONG content (4–5 wt.%) and low methanol content (0–0.29 wt.%). They have in common that their ashes are based on NaCl residues generated in the neutralization process with HCl. NaCl could be the main impurity responsible for the drop in catalytic activity.

Samples C and E present pH > 7, and their ashes are based on NaOH, which was used as a catalyst in the biodiesel synthesis, so that NaOH could be the main impurity responsible for the increase in conversion.

Sample B comes from the neutralization of sample C with formic acid, which leads to the formation of NaCOOH, and this presence of sodium formate would be responsible for the level of conversion achieved.

3.4.2. Stability and Reuse

Figure 6 shows the activity and selectivity results, obtained at 260 °C and 2 MPa H_2, using a 30 wt.% aqueous solution of analytical-grade glycerol (99.99%) as the reaction mixture. In the experiments, a ratio m_c/m_{gly} = 0.24 (mass ratio) was used in order to avoid oversizing, which would hide any deactivation. After each reaction test, the reactor is cooled, the liquid mixture (of products and reactants) is removed from the reactor and a new loading with a new 30 wt.% glycerol solution is performed.

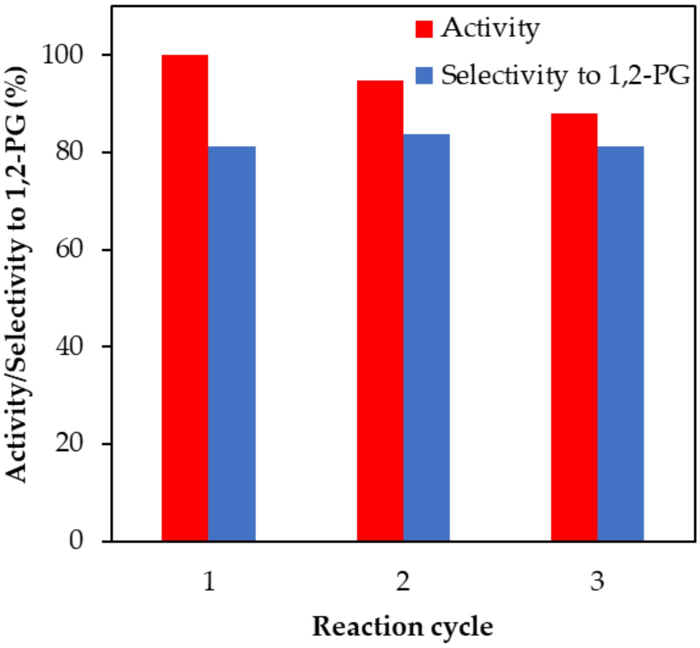

Figure 6. Reaction cycles for Ni/SC. Reaction conditions: 30 wt.% glycerol solution, 260 °C, 2 MPa H_2, 2 h, m_c/m_{gly} = 0.24 (mass ratio).

In Figure 6, it is shown that the Ni/SC catalyst at the end of the three activity tests loses only 12% of its initial conversion, while there are no significant changes in the selectivity to 1,2 PG. This is in agreement with the characterization results of the used Ni/SC catalyst (Table 1), which demonstrates that this sample retains the surface acidity of the support and the total number of acid sites.

Of all the crude glycerol samples studied, those with NaCl present (samples A and D) showed catalyst deactivation. Figure 7a shows the results obtained for sample D, which has the highest concentration of NaCl in crude glycerol. It is possible to observe a 75% drop in the initial activity of the catalyst after the third reaction cycle, together with a 25% drop in the selectivity to 1,2-PG.

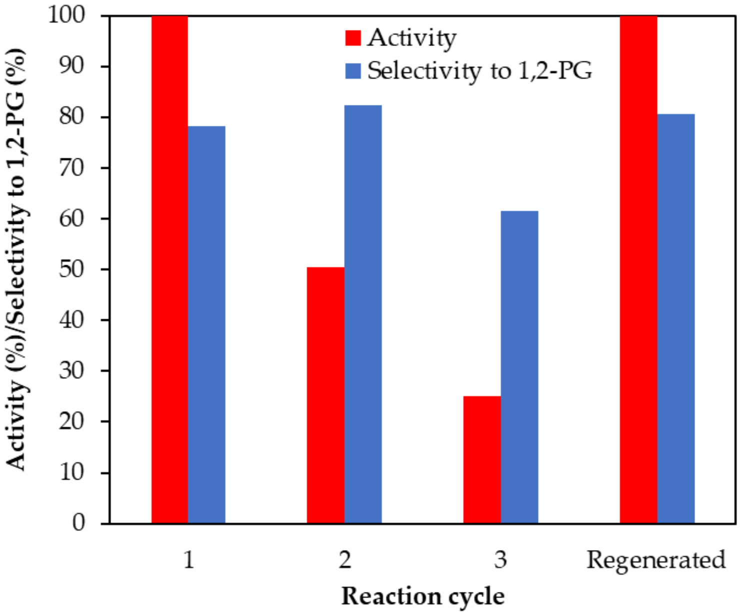

Figure 7. Activity and selectivity to 1,2-PG as a function of the reaction cycles for crude glycerol sample D. Reaction conditions: 30 wt.% glycerol solution, 260 °C, 2 MPa, m_c/m_{gly} = 0.24.

In order to identify the cause of NaCl deactivation over the catalyst, SEM-EDAX (Figure S5, Supplementary Materials) and XRD (Figure S6, Supplementary Materials) analyses were carried out and revealed the presence of Cl^- ions in the used catalyst after the third reaction cycle. To determine whether Cl^- ions can be removed from the solid, the used sample was washed with a solution of ethanol in water at room temperature, dried in a stove at 105 °C for 3 h and finally reduced in H_2 flow (50 $cm^3 min^{-1}$) at 400 °C for 90 min. The catalytic results shown in Figure 7 indicate that with this treatment the initial levels of activity and selectivity to1,2-PG are recovered, so that the presence of Cl^- in the solid is reversible and the catalyst used can be regenerated.

3.5. Kinetic Model Considering the Presence of Impurities in Crude Glycerol

Profiles of glycerol conversion and selectivity to liquid products as a function of temperature (Figure S7), H_2 partial pressure (Figure S8) and glycerol concentration (Figure S9) are presented in the Supplementary Materials.

Figure 8 shows a dotted line with the experimentally obtained results (at 260 °C and 2 MPa H_2, m_c/m_{gly} = 0.24 mass ratio and 30 wt.% analytical glycerol solutions); the solid line shows the variation in products and reactants when a power-law-based model is applied.

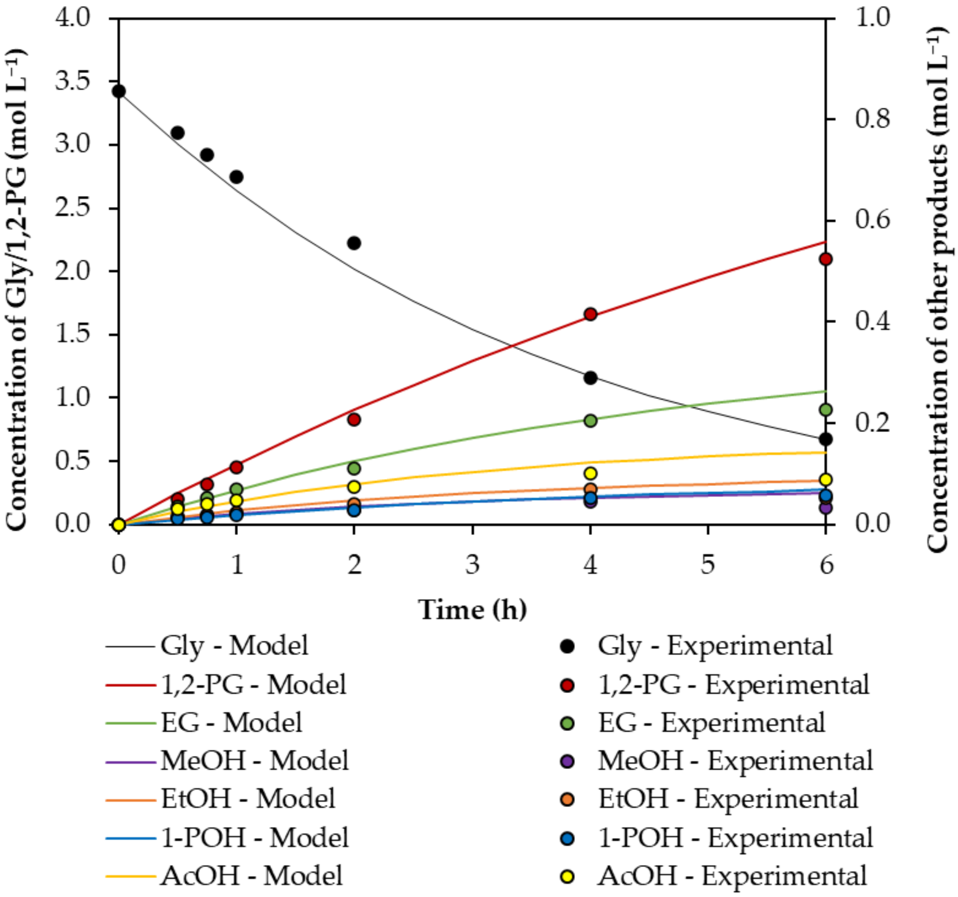

Figure 8. Concentration profiles as a function of time for glycerol and liquid products. Reaction conditions: 30 wt.% glycerol solution, 260 °C, 2 MPa, m_c/m_{gly} = 0.24.

The partial orders of reaction with respect to glycerol (α_j) and H_2 (β_j) and the kinetic constants (k_j), as well as the apparent activation energies (E_{aj}) and pre-exponential factors (k_{oj}), are shown in Tables 6 and 7. The adjustments are shown in the Supplementary Materials (Figures S10 and S11).

Table 6. Partial reaction orders with respect to glycerol (α_j) and H_2 (β_j) and the rates of glycerol consumption and product formation.

Compound	k_j ($mol^{1-\alpha-\beta}$ $L^{\alpha+\beta}$ g^{-1} s^{-1})	α_j	R^2 (α_j)	β_j	R^2 (β_j)
Gly	$9.64\ 10^{-7} \pm 8.78\ 10^{-8}$	0.95 ± 0.08	0.99	-	-
1,2-PG	$1.03\ 10^{-5} \pm 2.95\ 10^{-7}$	0.38 ± 0.03	0.99	0.45 ± 0.04	0.98
EG	$3.34\ 10^{-10} \pm 3.85\ 10^{-12}$	0.73 ± 0.01	0.99	-1.17 ± 0.16	0.96
AcOH	$1.28\ 10^{-10} \pm 3.53\ 10^{-12}$	1.21 ± 0.02	0.99	-0.97 ± 0.09	0.98
EtOH	$7.55\ 10^{-8} \pm 1.97\ 10^{-9}$	1.18 ± 0.02	0.99	0.22 ± 0.02	0.98
1-POH	$2.97\ 10^{-7} \pm 2.22\ 10^{-10}$	0.80 ± 0.02	0.99	0.49 ± 0.09	0.94
MeOH	$2.17\ 10^{-9} \pm 1.54\ 10^{-12}$	1.30 ± 0.08	0.99	-0.41 ± 0.05	0.97

Table 7. Fitted parameters of the Arrhenius equation: apparent activation energy (E_{aj}) and natural logarithm of the pre-exponential factor (k_{oj}) for the different compounds.

Compound (j)	ln (k_{oj})	E_{aj} (kJ mol^{-1})	R^2
Gly	18.68 ± 0.53	141.01 ± 2.28	0.99
1,2-PG	16.74 ± 1.33	124.66 ± 5.65	0.99
AcOH	26.45 ± 4.65	217.21 ± 19.81	0.97
EG	10.22 ± 0.48	141.08 ± 4.74	0.99
MeOH	30.62 ± 7.52	223.96 ± 32.01	0.94
EtOH	22.16 ± 5.06	171.24 ± 21.55	0.95
1-POH	8.80 ± 2.33	103.44 ± 9.94	0.97

Since no significant changes in the selectivity to liquid products were observed using crude glycerol samples, the kinetic model was modified to account for changes in conversion. For this purpose, the individual activity factors (a_i) were calculated from the ratio between the rate of glycerol consumption in the presence of the impurity ($-r_{gly}'$) and the rate of glycerol consumption in the absence of the impurity ($-r_{gly}$), using Equation (16). The individual activity factors (a_i) can be mathematically expressed as a function of the concentration of each impurity (C_i) from Equation (16).

The characteristic parameters of the individual activity factors (n, k_i, K_i) were obtained from the adjustment of the linearized Equation (16). The results of these parameters are shown in Table 8, and the adjustments are presented in the Supplementary Information (Figure S12).

Table 8. Characteristic parameters (n, k_i, K_i) of the individual activity factor (a_i).

Compound (i)	n	k_i (L^n mol^{-n})	K_i (L^n mol^{-n})	a_i	R^2
NaOH	2	72.37 ± 2.65	-	$1 + k_{NaOH}C_{NaOH}^2$	0.99
NaCOOH	2	53.09 ± 1.11	-	$1 + k_{NaCOOH}C_{NaCOOH}^2$	0.99
NaCl	1	31.25 ± 1.95	44.10 ± 1.23	$1 - \frac{k_{NaCl}C_{NaCl}}{1+K_{NaCl}C_{NaCl}}$	0.98
MeOH	2	2.76 ± 0.29	7.77 ± 0.37	$1 - \frac{k_{MeOH}C_{MeOH}^2}{1+K_{MeOH}C_{MeOH}^2}$	0.98

From the parameters shown in Table 8 and using Equation (17), the total activity factors (a_T) were calculated for each one of the crude glycerol samples (A–E). Based on the total activity factor, the glycerol consumption rate was expressed according to Equation (18), which was integrated to obtain the conversion values.

Figure 9 shows the conversion profiles as a function of time for the crude glycerol samples (A–E) and the conversion values experimentally measured versus those predicted by the model. The adjustment results indicate that the model allows for estimating the experimental conversions of the crude glycerol samples with an average error below 8%.

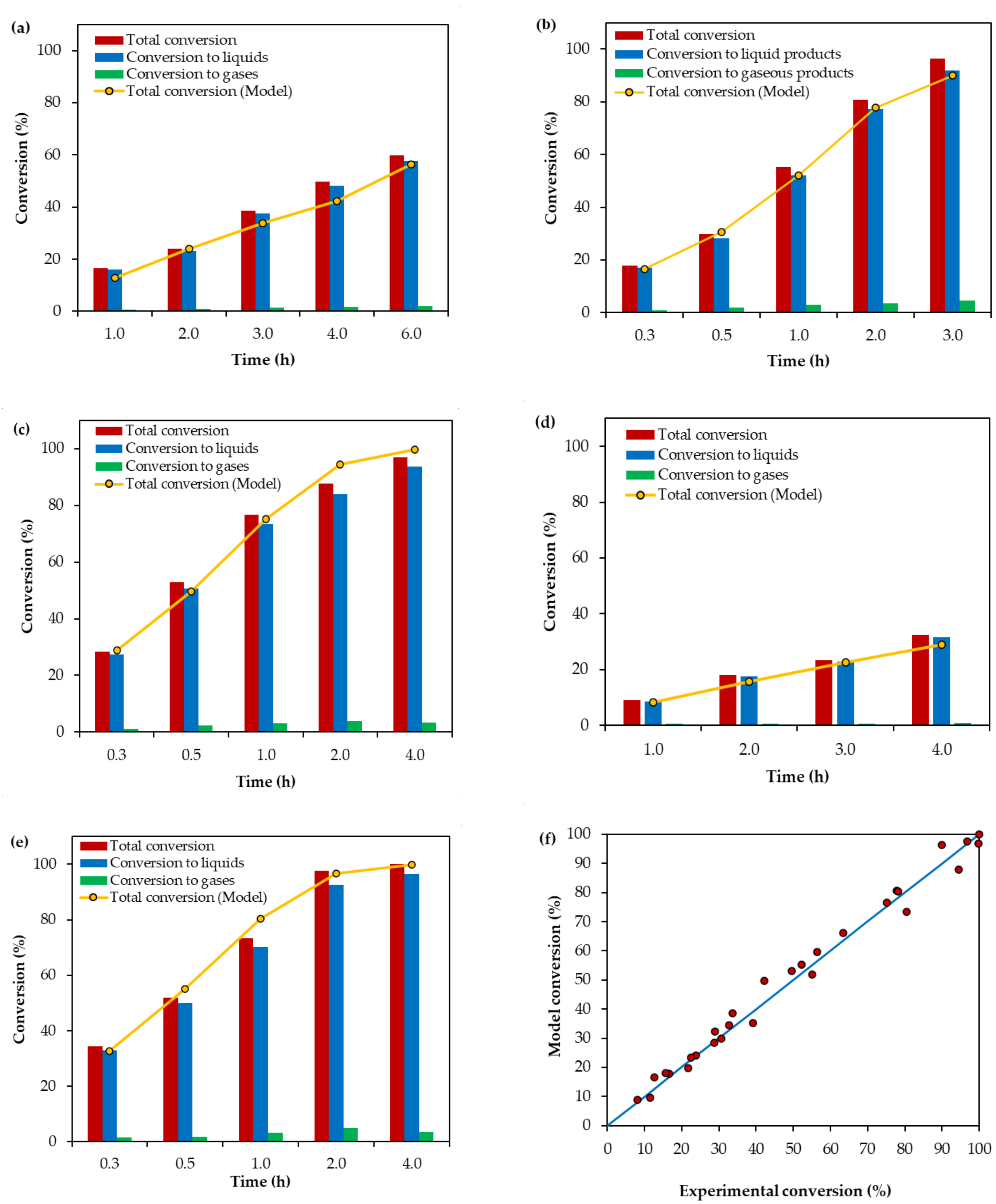

Figure 9. (**a**–**e**) Conversion as a function of time for crude glycerol samples A, B, C, D and E (**f**) Experimental conversion vs. model conversion. Reaction conditions: 30 wt.% glycerol solution, 260 °C, 2 MPa, m_c/m_{gly} = 0.24.

4. Conclusions

In this work, we studied the effect of the main impurities present in industrial crude glycerol samples on the activity, selectivity and stability of a Ni catalyst supported on a silica–carbon composite. The results obtained using glycerol of analytical grade (99% purity) allowed us to propose a kinetic model based on the power law that satisfactorily fitted the activity experimental results.

In order to determine the differences in activity using crude glycerol samples from different industries, the effect of each impurity over catalytic activity was examined. In this sense, the individual addition of each impurity determined that the presence of NaCl and MeOH negatively affects the catalytic activity, while the presence of NaOH and NaCOOH contributes to the reaction medium with OH^- groups that promote glycerol hydrogenolysis. On the other hand, the presence of H_2O does not affect the activity, due to the hydrophobic characteristics of the support and the presence of NaCl, which deactivates the catalyst in successive reaction cycles, but it is possible to regenerate it with a treatment of washing, drying and reduction in H_2 flow.

The calculation of individual activity factors for each impurity made it possible to modify the kinetic model so as to take into account the different compositions of industrial crude glycerol and to estimate catalytic activity with an average error below 8%.

Supplementary Materials: The following supporting information can be downloaded at: https://www.mdpi.com/article/10.3390/pr11061731/s1; Figure S1: N_2 adsorption–desorption isotherms of SC (●), Ni/SC (○) and Ni/SC* (▲); Figure S2: Potentiometric titration curves with n-butylamine in acetonitrile of SC (●), Ni/SC (○) and Ni/SC* (▲); Figure S3: TEM micrographs for the reduced catalysts (a) fresh Ni/SC (b) used Ni/SC*; Figure S4: XRD patterns of SC, Ni/SC reduced fresh catalyst and used Ni/SC* catalyst. Symbols are referred to metallic nickel (▲), silicon carbide (∆) and graphitic carbon (○); Figure S5: Analysis of elements by SEM-EDAX for the used catalyst after three reaction cycles in the presence of the crude glycerol sample D. Reaction conditions: 30 wt.% aqueous glycerol solution, 260 °C, 2 MPa, 2 h, mc/mgly = 0.24 (mass ratio); Figure S6: XRD patterns of Ni/SC reduced fresh catalyst and used Ni/SC* catalyst. Symbols are referred to planes (2 0 0) at 31.69° and (2 2 0) at 45.45° of crystalline cubic NaCl (⧫) (JCPDS 05-0628); Figure S7: (a) Glycerol conversion vs. temperature (b) Selectivity to liquid products vs. temperature. Reaction conditions: 30 wt.% aqueous glycerol solution, 2 h, 2 MPa H_2, $m_c/m_{gly} = 0.24$ (mass ratio); Figure S8: (a) Glycerol conversion vs. partial pressure of H_2 (b) Selectivity to liquid products vs. partial pressure of H_2. Reaction conditions: 30 wt.% aqueous glycerol solution, 260 °C, 2 h, $m_c/m_{gly} = 0.24$ (mass ratio); Figure S9: (a) Glycerol conversion vs. glycerol initial concentration (b) Selectivity to liquid products vs. initial glycerol concentration. Reaction conditions: 30–80 wt.% aqueous glycerol solutions, 260 °C, 2 MPa de H_2, 2 h, $m_c/m_{gly} = 0.08$–0.24 (mass ratio); Figure S10: Fitting of experimental data by linear regression to obtain the reaction orders with respect to glycerol and hydrogen for (a) Gly (b, b′) 1,2-PG (c, c′) AcOH (d, d′) EG (e, e′) MeOH (f, f′) EtOH (g, g′) 1-POH. Reaction conditions: 30 wt.% aqueous glycerol solution, 260 °C, 1–2 MPa H_2, 0.5–1 h, $m_c/m_{gly} = 0.24$ (mass ratio); Figure S11: Fitting of experimental data by linear regression to obtain ln (k_{oj}) y Ea_j (a) Gly (b) 1,2-PG (c) AcOH (d) EG (e) MeOH (f) EtOH (g) 1-POH. Reaction conditions: 30 wt.% aqueous glycerol solution, 220–260 °C, 2 MPa H_2, 2 h, $m_c/m_{gly} = 0.24$ (mass ratio); Figure S12: Fitting of experimental data by linear regression to obtain the individual activity factors (a_i) for (a) NaOH (b) NaCOOH (c) NaCl (d) MeOH. Reaction conditions: 30 wt.% aqueous glycerol solution, 260 °C, 2 MPa H_2, 2 h, $m_c/m_{gly} = 0.24$ (mass ratio).

Author Contributions: Conceptualization, M.N.G. and N.N.N.; methodology, M.N.G., G.F.S. and F.P.; software, M.N.G.; validation, F.P., G.F.S. and N.N.N.; formal analysis, M.N.G.; investigation, M.N.G.; resources, N.N.N.; data curation, N.N.N. and G.F.S.; writing—original draft preparation, M.N.G. and N.N.N.; writing—review and editing, M.N.G., G.F.S. and N.N.N.; visualization, M.N.G. and G.F.S.; supervision, F.P. and N.N.N.; project administration, N.N.N.; funding acquisition, N.N.N. and G.F.S. All authors have read and agreed to the published version of the manuscript.

Funding: This research was funded by CONICET, grant number PIP 0065, and UNLP, grant number I-248.

Data Availability Statement: Data reported were taken from papers included in the references.

Acknowledgments: This research work was possible due to the funds received from "Consejo Nacional de InvestigacionesCientíficas y Técnicas" (CONICET-PIP 0065), "Universidad Nacional de La Plata" (UNLP-I248). Martín N. Gatti thanks UNLP for awarding him the Young Researchers Grant (7207/19).

Conflicts of Interest: The authors declare no conflict of interest.

References

1. Guo, M.; Song, W.; Buhain, J. Bioenergy and biofuels: History, status, and perspective. *Renew. Sustain. Energy Rev.* **2015**, *42*, 712–725. [CrossRef]
2. Wang, Y.; Xiao, Y.; Xiao, G. Sustainable value-added C3 chemicals from glicerol transformations: A mini review for heterogeneous catalytic processes. *Chin. J. Chem. Eng.* **2019**, *27*, 1536–1542. [CrossRef]
3. Gatti, M.N.; Perez, F.M.; Santori, G.F.; Nichio, N.N.; Pompeo, F. Heterogeneous Catalysts for Glycerol Biorefineries: Hydrogenolysis to 1,2-Propylene Glycol. *Materials* **2023**, *16*, 3551. [CrossRef] [PubMed]
4. Dasari, M.A.; Kiatsimkul, P.-P.; Sutterlin, W.R.; Suppes, G.J. Low-pressure hydrogenolysis of glicerol to propyleneglycol. *Appl. Catal. A Gen.* **2005**, *281*, 225–231. [CrossRef]
5. Miyazawa, T.; Kusunoki, Y.; Kunimori, K.; Tomishige, K. Glycerol conversion in theaqueous solution under hydrogen over Ru/C + an ion-exchange resin and its reaction mechanism. *J. Catal.* **2006**, *240*, 213–221. [CrossRef]
6. Li, K.-T.; Yen, R.-H. Aqueous-Phase Hydrogenolysis of Glycerol over Re Promoted Ru Catalysts Encapuslated in Porous Silica Nanoparticles. *Nanomaterials* **2018**, *8*, 153. [CrossRef]
7. Checa, M.; Montes, V.; Hidalgo-Carrillo, J.; Marinas, A.; Urbano, F.J. Influence of Boron, Tungsten and Molybdenum Modifiers on Zirconia Based Pt Catalyst for Glycerol Valorization. *Nanomaterials* **2019**, *9*, 509. [CrossRef]
8. Kim, N.D.; Park, J.R.; Park, D.S.; Kwak, B.K.; Yi, J. Promoter effect of Pd in $CuCr_2O_4$catalysts on the hydrogenolysis of glycerol to 1,2-propanediol. *Green Chem.* **2012**, *14*, 2638–2646. [CrossRef]
9. Pandhare, N.N.; Pudi, S.M.; Mondal, S.; Pareta, K.; Kumar, M.; Biswas, P. Development of Kinetic Model for Hydrogenolysis of Glycerol over Cu/MgO Catalyst in a Slurry Reactor. *Ind. Eng. Chem. Res.* **2018**, *57*, 101–110. [CrossRef]
10. Grabysch, T.; Muhler, M.; Peng, B. The kinetics of glycerol hydrodeoxygenation to 1,2-propanediol over Cu/ZrO_2 in the aqueous phase. *Appl. Catal. A Gen.* **2019**, *576*, 47–53. [CrossRef]
11. Mondal, S.; Malviya, H.; Biswas, P. Kinetic modelling for the hydrogenolysis of bio-glycerol in the presence of a highly selective $Cu\text{-}Ni\text{-}Al_2O_3$ catalyst in a slurry reactor. *React. Chem. Eng.* **2019**, *4*, 595–609. [CrossRef]
12. Gatti, M.N.; Pompeo, F.; Santori, G.F.; Nichio, N.N. High Yield to 1-Propanol from Crude Glycerol Using Two Reaction Steps with Ni Catalysts. *Catalysts* **2020**, *10*, 615. [CrossRef]
13. Vasiliadou, E.S.; Lemonidou, A.A. Kinetic study of liquid-phase glycerol hydrogenolysis over Cu/SiO_2 catalyst. *Chem. Eng. J.* **2013**, *231*, 103–112. [CrossRef]
14. Rekha, V.; Raju, N.; Sumana, C.; Douglas, S.P.; Lingaiah, N. Selective Hydrogenolysis of Glycerol Over $Cu\text{-}ZrO_2\text{-}MgO$ Catalysts. *Catal. Lett.* **2016**, *146*, 1487–1496. [CrossRef]
15. Rekha, V.; Sumana, C.; Douglas, S.P.; Lingaiah, N. Understanding the role of Co in Co–ZnO mixed oxide catalysts for the selective hydrogenolysis of glycerol. *Appl. Catal. A Gen.* **2015**, *491*, 155–162. [CrossRef]
16. Torres, A.; Roy, D.; Subramaniam, B.; Chaudhari, R.V. Kinetic Modeling of Aqueous-Phase Glycerol Hydrogenolysis in a Batch Slurry Reactor. *Ind. Eng. Chem. Res.* **2010**, *49*, 10826–10835. [CrossRef]
17. Lahr, D.G.; Shanks, B.H. Kinetic Analysis of the Hydrogenolysis of Lower Polyhydric Alcohols: Glycerol to Glycols. *Ind. Eng. Chem. Res.* **2003**, *42*, 5467–5472. [CrossRef]
18. Lahr, D.G.; Shanks, B.H. Effect of sulfur and temperature on ruthenium-catalyzed glycerol hydrogenolysis to glycols. *J. Catal.* **2005**, *232*, 386–394. [CrossRef]
19. Xi, Y.; Holladay, J.E.; Frye, J.G.; Oberg, A.A.; Jackson, J.E.; Miller, D.J. A Kinetic and Mass Transfer Model for Glycerol Hydrogenolysis in a Trickle-Bed Reactor. *Org. Process Res. Dev.* **2010**, *14*, 1304–1312. [CrossRef]
20. Sharma, R.V.; Kumar, P.; Dalai, A.K. Selective hydrogenolysis of glycerol to propylene glycol by using Cu:Zn:Cr:Zr mixed metal oxides catalyst. *Appl. Catal. A Gen.* **2014**, *477*, 147–156. [CrossRef]
21. Jin, X.; Subramaniam, B.; Chaudhari, R.V. Kinetic modeling of Pt/C catalyzed aqueous phase glycerol conversion with in situ formed hydrogen. *AIChE J.* **2016**, *62*, 1162–1173. [CrossRef]
22. Gandarias, I.; Fernández, S.G.; Doukkali, M.E.; Requies, J.; Arias, P.L. Physicochemical Study of Glycerol Hydrogenolysis Over a $Ni\text{-}Cu/Al_2O_3$ Catalyst Using Formic Acid as the Hydrogen Source. *Top. Catal.* **2013**, *56*, 995–1007. [CrossRef]
23. Tao, J.; Meixuan, R.; Shishi, C.; Qiang, H.; Weiyong, Y.; Fahai, C. Kinetics of Hydrogenolysis of Glycerol to Ethylene Glycol over Raney Ni Catalyst. *Adv. Mater. Res.* **2014**, *906*, 103–111. [CrossRef]
24. Zhou, Z.; Li, X.; Zeng, T.; Hong, W.; Cheng, Z.; Yuan, W. Kinetics of Hydrogenolysis of Glycerol to Propylene Glycol over $Cu\text{-}ZnO\text{-}Al_2O_3$ Catalysts. *Chin. J. Chem. Eng.* **2010**, *18*, 384–390. [CrossRef]
25. Balaraju, M.; Rekha, V.; Prabhavathi Devi, B.L.A.; Prasad, R.B.N.; Sai Prasad, P.S.; Lingaiah, N. Surface and structural properties of titania-supported Ru catalysts for hydrogenolysis of glycerol. *Appl. Catal. A Gen.* **2010**, *384*, 107–114. [CrossRef]

26. Zhu, S.; Zhu, Y.; Hao, S.; Zheng, H.; Mo, T.; Li, Y. One-step hydrogenolysis of glycerol to biopropanols over Pt–$H_4SiW_{12}O_{40}/ZrO_2$ catalysts. *Green Chem.* **2012**, *14*, 2607–2616. [CrossRef]
27. Rajkhowa, T.; Marin, G.B.; Thybaut, J.W. Quantifying the dominant factors in Cu catalyst deactivation during glycerol hydrogenolysis. *J. Ind. Eng. Chem.* **2017**, *54*, 270–277. [CrossRef]
28. Nanda, M.R.; Yuan, Z.; Shui, H.; Xu, C. Selective Hydrogenolysis of Glycerol and Crude Glycerol (a By-Product or Waste Stream from the Biodiesel Industry) to 1,2-Propanediol over B_2O_3 Promoted Cu/Al_2O_3 Catalysts. *Catalysts* **2017**, *7*, 196. [CrossRef]
29. Mane, R.B.; Rode, C.V. Simultaneous glycerol dehydration and in situ hydrogenolysis over Cu–Al oxide under an inert atmosphere. *Green Chem.* **2012**, *14*, 2780–2789. [CrossRef]
30. Maris, E.P.; Davis, R.J. Hydrogenolysis of Glycerol over Carbon-Supported Ru and Pt Catalysts. *J. Catal.* **2007**, *249*, 328–337. [CrossRef]
31. Balaraju, M.; Jagadeeswaraiah, K.; Sai Prasad, P.S.; Lingaiah, N. Catalytic hydrogenolysis of biodiesel derived glycerol to 1,2-propanediol over Cu–MgO catalysts. *Catal. Sci. Technol.* **2012**, *2*, 1967–1976. [CrossRef]
32. Gandarias, I.; Arias, P.L.; Fernandez, S.G.; Requies, J.; Doukkali, M.E.; Guemez, M.B. Hydrogenolysis through catalytic transfer hydrogenation: Glycerol conversion to 1,2-propanediol. *Catal. Today* **2012**, *195*, 22–31. [CrossRef]
33. Cai, F.; Song, X.; Wu, Y.; Zhang, J.; Xiao, G. Selective Hydrogenolysis of Glycerol over Acid-Modified Co–Al Catalysts in a Fixed-Bed Flow Reactor. *ACS Sustain. Chem. Eng.* **2018**, *6*, 110–118. [CrossRef]
34. Gatti, M.N.; Mizrahi, M.D.; Ramallo-Lopez, J.M.; Pompeo, F.; Santori, G.F.; Nichio, N.N. Improvement of the catalytic activity of Ni/SiO_2-C by the modification of the support and Zn addition: Bio-propyleneglycolfrom glycerol. *Appl. Catal. A Gen.* **2017**, *548*, 24–32. [CrossRef]
35. Gatti, M.N.; Pompeo, F.; Santori, G.F.; Nichio, N.N. Bio-propylene glycol by liquid phase hydrogenolysis of glicerol with Ni/SiO_2-C catalysts. *Catal. Today* **2017**, *296*, 26–34. [CrossRef]
36. Xia, S.; Yuan, Z.; Wang, L.; Chen, P.; Hou, Z. Catalytic production of 1,2-propanediol from glycerol in bio-ethanol solvent. *Bioresour. Technol.* **2012**, *104*, 814–817. [CrossRef]
37. Menchavez, R.N.; Morra, M.J.; He, B.B. Co-Production of Ethanol and 1,2-Propanediol via Glycerol Hydrogenolysis Using Ni/Ce–Mg Catalysts: Effects of Catalyst Preparation and Reaction Conditions. *Catalysts* **2017**, *7*, 290. [CrossRef]
38. Kusonoki, Y.; Miyazawa, T.; Kunimori, K.; Tomishige, K. Highly active metal–acid bifunctional catalyst system for hydrogenolysis of glycerol under mild reaction conditions. *Catal. Commun.* **2005**, *6*, 645–649. [CrossRef]
39. Maglinao, R.L.; He, B.B. Verification of Propylene Glycol Preparation from Glycerol via the Acetol Pathway by in Situ Hydrogenolysis. *Biofuels* **2012**, *3*, 675–682. [CrossRef]
40. Feng, J.; Wang, J.; Zhou, Y.; Fu, H.; Chen, H.; Li, X. Effect of Base Additives on the Selective Hydrogenolysis of Glycerol over Ru/TiO_2 Catalyst. *Chem. Lett.* **2007**, *36*, 1274–1275. [CrossRef]
41. Marinoiu, A.; Cobzaru, C.; Carcadea, E.; Capris, C.; Tanislav, V.; Raceanu, M. Hydrogenolysis of glycerol to propylene glycol using heterogeneous catalysts in basic aqueous solutions. *React. Kinet. Mech. Catal.* **2013**, *110*, 63–73. [CrossRef]
42. Boga, D.A.; Liu, F.; Bruijnincx, P.C.A.; Weckhuysen, B.M. Aqueous-phase reforming of crude glycerol: Effect of impurities on hydrogen production. *Catal. Sci. Technol.* **2016**, *6*, 134. [CrossRef]
43. Lehnert, K.; Claus, P. Influence of Pt particle size and support type on the aqueous-phase reforming of glycerol. *Catal. Commun.* **2008**, *9*, 2543–2546. [CrossRef]
44. Zhou, C.H.; Deng, K.; Di Serio, M.; Xiao, S.; Tong, D.S.; Li, L.; Lin, C.X.; Beltramini, J.; Zhang, H.; Yu, W.H. Cleaner hydrothermal hydrogenolysis of glycerol to 1,2-propanediol over Cu/oxide catalysts without addition of external hydrogen. *Mol. Catal.* **2017**, *432*, 274–284. [CrossRef]